

Communication

Characterization and Structural Insights of a Novel Arylsulfatase from *Pseudoalteromonas atlantica* T6c

Panpan Dong^{1,†}, Wendi Yang^{2,†} , Lifang Sun¹, Dingding Jing¹, Hong Zhang¹, Jinbo Yang¹, Linjiao Wu¹, Leiqing Chen¹ and Yunkun Wu^{1,*}

¹ Provincial University Key Laboratory of Cellular Stress Response and Metabolic Regulation, College of Life Science, Fujian Normal University, Fuzhou 350117, China

² Fujian Metrology Institute, Fuzhou 350003, China

* Correspondence: wuyk@fjnu.edu.cn

† These authors contributed equally to this work.

Abstract: Arylsulfatases exhibit great potential in industry for desulfation applications, but less is known about the metallo- β -lactamase (MBL) fold arylsulfatases. To learn more about them, an MBL fold arylsulfatase from *Pseudoalteromonas atlantica* T6c (PaAst) was identified and characterized, and its structure was elaborated in this study. PaAst was sequence analyzed, heterologously expressed in *E. coli*, purified by Ni²⁺-NTA resin affinity chromatography and size-exclusion chromatography, functionally studied by *p*-nitrophenyl sulfate (*p*NPS), and crystallized for structure determination. The MBL fold arylsulfatase was identified by sequence analysis and confirmed by enzymatic assay on *p*NPS with K_m 1.00 mM and V_{max} 60.80 U/mg at 50 °C and pH 7.5. Furthermore, its crystals were obtained in 0.2 M sodium thiocyanate, 20% PEG3350, and its structure was determined at 2.0 Å that formed a dimer with MBL fold. Our work highlighted the MBL fold arylsulfatases from structural insights and could be the theoretical foundation for investigations into their catalytic mechanism.

Keywords: MBL-fold; arylsulfatase; crystallization; structure



Citation: Dong, P.; Yang, W.; Sun, L.; Jing, D.; Zhang, H.; Yang, J.; Wu, L.; Chen, L.; Wu, Y. Characterization and Structural Insights of a Novel Arylsulfatase from *Pseudoalteromonas atlantica* T6c. *Catalysts* **2023**, *13*, 759. <https://doi.org/10.3390/catal13040759>

Academic Editor: Evangelos Topakas

Received: 23 March 2023

Revised: 11 April 2023

Accepted: 12 April 2023

Published: 15 April 2023



Copyright: © 2023 by the authors. Licensee MDPI, Basel, Switzerland. This article is an open access article distributed under the terms and conditions of the Creative Commons Attribution (CC BY) license (<https://creativecommons.org/licenses/by/4.0/>).

1. Introduction

Sulfatase (EC 3.1.6.X) is a large family of hydrolytic enzymes found in various species, ranging from bacteria to humans, catalyzing the hydrolysis of sulfate ester bonds [1–3]. It has been classified into three distinct types, with the best studied, type I, identified as the C α -formylglycine-dependent arylsulfatases characterized by a unique formylglycine (FGly) posttranslationally modified from an active-site serine or cysteine [2,4,5]. The sulfatases (type II) consist of the Fe²⁺ α -ketoglutarate-dependent deoxygenate superfamily that require α -ketoglutarate as a cosubstrate [6–8], while the type III sulfatases were not reported until Hagelueken et al., in 2006, determined the crystal structure of SdsA1, a metallo- β -lactamase (MBL)-related alkylsulfatase from *Pseudomonas aeruginosa* [4]. Since then, a variety of MBL fold alkylsulfatases had been classified into sulfatases (type III), for example, SdsA from *Pseudomonas* sp. ATCC19151 [9], SdsAP from *Pseudomonas* sp. S9 [2,10], and Pisa1 from *Pseudomonas* sp. DSM6611 [11]. However, evidence also exists for the arylsulfatases sharing MBL fold, implicating AtsA from *Pseudoalteromonas carrageenovora* and a series of AtsA-like arylsulfatases [3,12–14]. Until now, this type of arylsulfatases could not be classified.

MBL fold sulfatases regulate the sulfation states of substrates, and it is suggested that sulfatases (type III) can degrade sodium dodecyl sulfate (SDS), with SdsA1 allowing its hosts to use SDS as a sole carbon or sulfur source [2,4,10]. SDS has been extensively used as an anionic surfactant in industries and daily life, which may cause secondary pollution to the environment [2,15]. Agar and its important component, agarose, have also been widely used in food, cosmetic, biological and pharmaceutical industries, and the removal of their sulfate groups by arylsulfatases could improve the gelling strength and purity

greatly [13,16]. AtsA and its homologous arylsulfatase, PfAST from *Pyrococcus furiosus* DSM3638, have been proven to exhibit activities towards an artificial aromatic sulfate, *p*-nitrophenyl sulfate (*p*NPS), and sulfated marine polysaccharide, agar [14]. Therefore, microbial MBL fold sulfatases are of great industrial interest due to their potential in the biodegradation of SDS and desulfation of marine sulfonated polysaccharides that could be environmental friendly and cost saving with less chemical solvents and reduced waste discharge [10,13,14,17].

Several investigations have been done to determine the structures of type III alkylsulfatases, and the MBL fold proteins exhibit diverse features [10,18]. SdsA1, SdsAP, and Pisa1 share a similar overall structure consisting of an MBL fold domain, a dimerization domain, and a sterol carrier protein type 2 (SCP-2)-like fold domain; however, SdsA1 and SdsAP are primary alkylsulfatases capable of hydrolyzing the primary alkyl sulfates, for example, SDS, while Pisa1 is a secondary alkylsulfatase hydrolyzing the secondary alkyl sulfates, such as *rac*-2-octyl sulfate [4,10,11]. The difference could be attributed to the structure of their active site regions. Studies on MBL fold arylsulfatases have focused on their enzymatic characteristics and engineering in the past decades, for example AtsA [3,12–14], but limited structural information was found. Structural analyses of them were based on structure homology modelling. Furthermore, it has long been assumed that all arylsulfatases belong to the type I arylsulfatases containing a conserved FGly motif with few exceptions [12,19], ignoring the AtsA-like arylsulfatases. The catalytic mechanism of these arylsulfatases was uncertain.

For better knowledge and application of arylsulfatases, further investigations were necessary from genetic, biochemical, and, more importantly, structural aspects. In this study, we identified a novel MBL fold arylsulfatase from a deep-sea agar-degrading bacterium, *Pseudoalteromonas atlantica* T6c, designated as PaAst, and its functional and structural analyses were conducted preliminarily.

2. Results and Discussion

2.1. Sequence Analysis of PaAst

Pseudoalteromonas atlantica T6c (GenBank: CP000388.1) is an agar-degrading bacterium isolated from marine environments and is likely to harbor arylsulfatase genes. In its complete genome, a 987 bp gene was predicted to encode a β -lactamase-like protein of 328 amino acids, with an estimated molecular weight of 35.6 kDa and a theoretical pI of 5.77 [20]. The protein was predicted to possess an N-terminal signal peptide of 22 amino acids with the cleavage site between residues Ala22 and Asp23 [21]. The sequence alignment through BLAST revealed relatively high identities between PaAst and its homologues; 14 MBL-fold metallo-hydrolases and 1 arylsulfatase exhibited identities higher than 60%. The highest identity, 70.68%, was carried out by an MBL fold metallo-hydrolase from *Shewanella* sp. UCD-KL21 (Sequence ID: WP_083698034.1, E value: 1e-160, coverage: 93%), and PaAst showed identities of 67.07%, 66.77%, and 65.55% to similar hydrolases in *Alteromonas stellipolaris* (Sequence ID: WP_062086863.1, E value: 2e-167), *Alteromonas* sp. MMG017 (Sequence ID: WP_211069552.1, E value: 1e-160), and *Paraglaciecola hydrolytica* (Sequence ID: WP_082769068.1, E value: 9e-168) with 100% coverage, respectively. Moreover, it is a homologue of the arylsulfatase AtsA.

PaAst is a member of the metallo-hydrolase-like MBL-fold superfamily that is highly homologous to AtsA (sequence identity: 60.06%), as well as the starting model for structure determination, YhfI, from *Bacillus subtilis* (Figure 1). The homologues harbor conserved Zn²⁺-binding motifs, as “SH × H × DH-H181-D213-H289” in PaAst. In addition to its close identity with AtsA, its only domain, from Glu31 to Ser232, is a conserved arylsulfatase AtsA-like MBL-fold domain (Accession no. cd07719) [22,23]. Accordingly, although the conserved FGly motif (C/S × A/P × R) of arylsulfatases could not be found in its sequence, PaAst has a definite possibility of functioning as the arylsulfatases AtsA and PfAST, which could be confirmed in the following enzymatic assays.

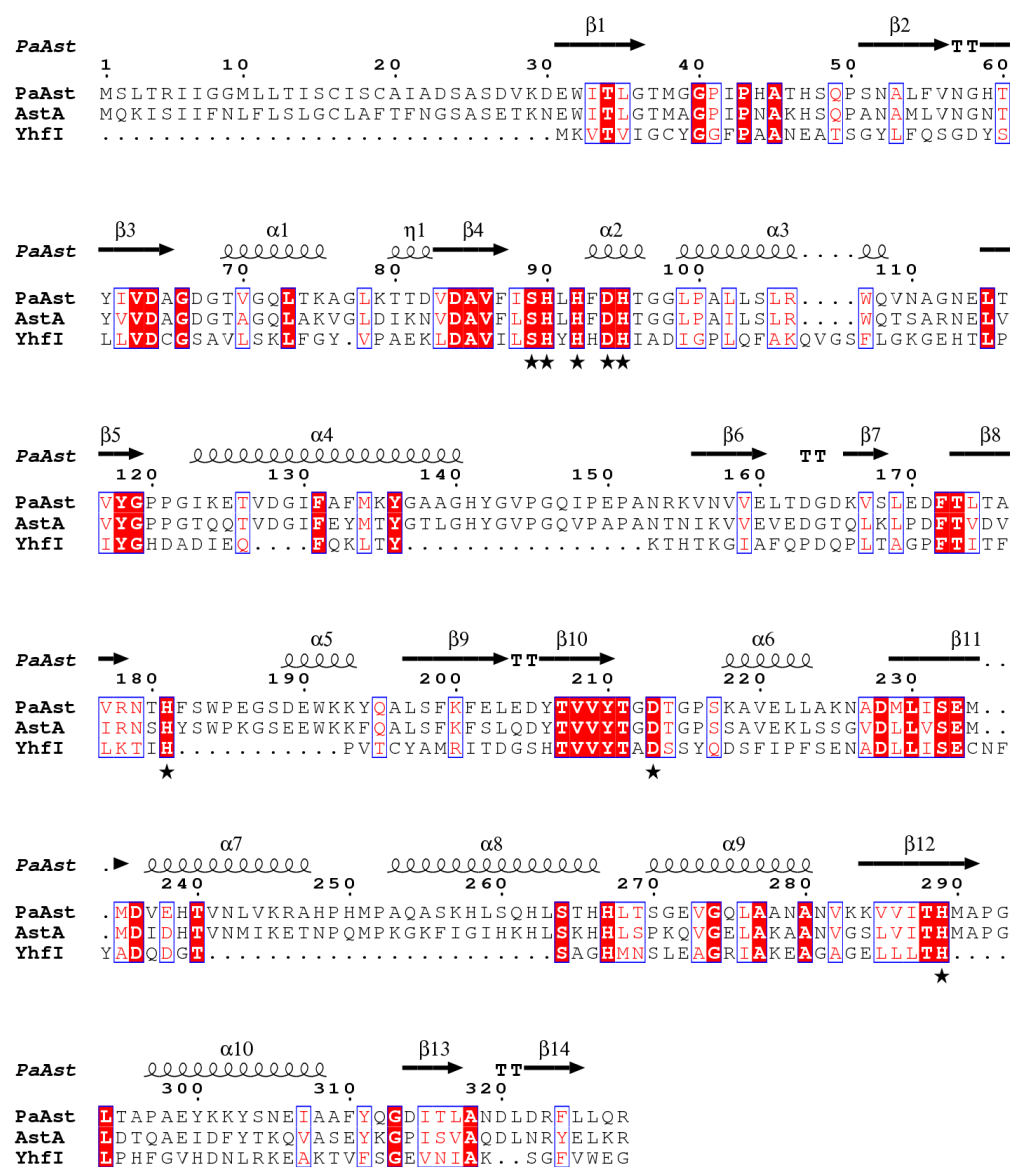


Figure 1. Sequence alignment of PaAst (GenBank: ABG39403.1), AtsA (GenBank: CAA46628.1), and YhfI (GenBank: ADM37089.1). Identical residues are highlighted in red, similar residues are framed in blue, and residues in the conserved Zn²⁺-binding motifs are labeled with stars.

2.2. Expression, Purification, and Characterization of Recombinant PaAst

Recombinant PaAst was constructed, heterologously expressed, and purified for the confirmation of its enzymatic activity against *pNPS* and subsequent crystallization. The codon-optimized and truncated *PaAst* gene was inserted into the pET32a expression system, transformed into *E. coli* BL21 (DE3), and expressed as a PaAst-6*His-Trx fusion protein at a high level. To maintain its bioactivity, the purification mainly consisted of two rounds of Ni²⁺ affinity chromatography, and the size-exclusion chromatography, was conducted at low temperatures. The calculated molecular weight should have been 34.2 kDa for the purified recombinant enzyme after the 6*His-Trx tag removed, which was consistent with the SDS-PAGE analysis shown in Figure 2. However, in the size-exclusion chromatography, elution volume for the recombinant PaAst was 14.85 mL, indicating a molecular weight close to 75 kDa, appropriately twice the molecular weight of the monomer, indicating that PaAst is a dimer in solution.

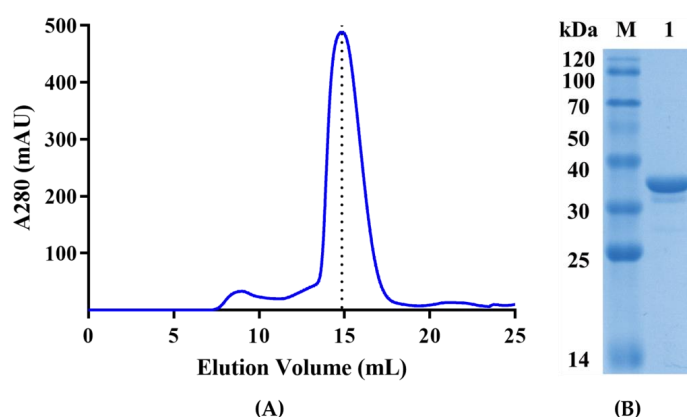


Figure 2. Purification of PaAst. (A) Size-exclusion chromatography of recombinant PaAst. The elution volume was 14.85 mL, between standard samples ovalbumin (44 KD) and conalbumin (75 KD), and closer to conalbumin. (B) SDS-PAGE analysis of the purified recombinant PaAst. Lane M, protein marker; Lane 1, purified recombinant PaAst.

Recombinant PaAst was enzymatically active towards *p*NPS, a common artificial substrate to evaluate enzymatic activities of the arylsulfatases [12]. The purification yields of PaAst are shown in Table 1 after procedures of crude extraction, Ni²⁺ affinity chromatography, and size-exclusion chromatography. After the steps of Ni²⁺ affinity chromatography, dialysis, and a secondary Ni²⁺ affinity chromatography, the total protein decreased from 220.32 mg to 22.93 mg, but the specific activity increased by three folds. The size-exclusion chromatography had less effect on the activity than the former steps, and the final yield for purification was 14.76%. The final yield and purification factor for PaAst were higher than AtsA heterologous expressed in *E. coli* performed with the same procedures in the same conditions (Table A2). The specific activity of purified PaAst on *p*NPS was 39.45 U/mg at 50 °C. The kinetic parameters were also obtained at 50 °C by exhibiting a Michaelis–Menten plot with specific activities on different concentrations of *p*NPS (Figure 3). The purified recombinant PaAst was observed with K_m and V_{max} of 1.00 mM and 60.80 U/mg, respectively. The results demonstrated that PaAst could hydrolyze *p*NPS efficiently, indicating its belonging to the arylsulfatase family.

Table 1. Purification yields of recombinant PaAst.

Purification Procedures	Total Protein (mg)	Total Activity (U)	Specific Activity (U/mg)	Purification Factor	Yield (%)
Crude extract	220.32	2613.00	11.86	1	100
Affinity chromatography	22.93	840.21	36.64	3.08	32.16
Size-exclusion chromatography	9.77	385.62	39.45	3.33	14.76

Enzymatic activities were determined by *p*NPS in 50 mM Tris-HCl (pH 7.5) buffer at 50 °C.

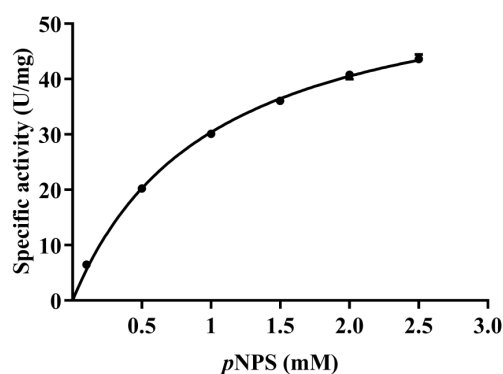


Figure 3. Specific activity of PaAst towards *p*NPS. Some error bars could not be seen.

2.3. Crystal Structure of PaAst

Purified recombinant PaAst was crystallized in various conditions, but the majority obtained were needle-like crystals. Fortunately, slice-like diffraction-quality crystals grew in 0.2 M sodium thiocyanate and 20% PEG3350 at 16 °C (Figure 4), and PEG400 was selected as the cryoprotectant. PaAst was crystallized in space group $P 1 2_1 1$ with its unit cell parameters $a = 55.17 \text{ \AA}$, $b = 61.38 \text{ \AA}$, $c = 89.60 \text{ \AA}$, $\alpha = 90^\circ$, $\beta = 97.88^\circ$, and $\gamma = 90^\circ$, and the diffraction and refinement statistics are summarized in Table A1. The X-ray diffraction data were collected in a resolution range of 38.61–1.55 \AA , and the final structure was determined at 2.0 \AA with R_{work} of 20.04% and R_{free} of 24.35% by molecular replacement. A comparison of protein structures through the Dali server indicated that the closest homologue of PaAst was chain A of *Bacillus subtilis* Ribonuclease Z (RNase Z, PDB: 4GCW), a member of the β -lactamase family, sharing a Z-score of 32.9 with a sequence identity of 27% and an RMSD of 2.1 \AA [24,25]. The starting model, Yhfl, also exhibited an extensive homology to PaAst, with a Z-score of 29.1, sequence identity of 21%, and RMSD of 1.9 \AA .

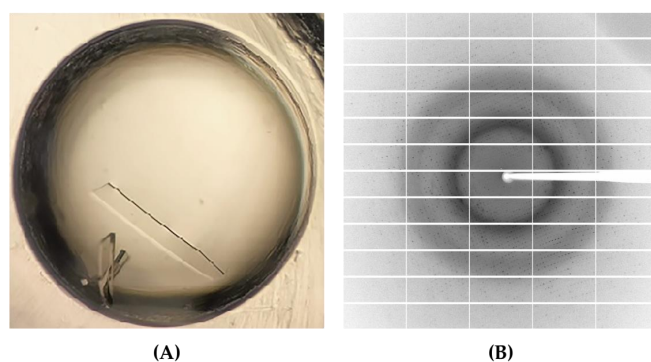


Figure 4. Crystallization and X-ray diffraction of PaAst. (A) Crystals observed in 0.2 M sodium thiocyanate, 20% PEG3350. (B) Representative diffraction pattern.

Each asymmetric unit contained two chains of PaAst sharing RMSD of 0.18 \AA over $C\alpha$, and the chains formed a dimer with extensive contacts (Figure 5A). According to the calculation of the PDBe PISA Server (https://www.ebi.ac.uk/msd-srv/prot_int/cgi-bin/piserver, accessed on 19 September 2022), the dimer interface had a buried solvent accessible area of 2245.3 \AA^2 , which accounted for 16.5% of the total solvent accessible area. Therefore, the dimerization could be observed both in solution, proved by size-exclusion chromatography, and in the crystal structure.

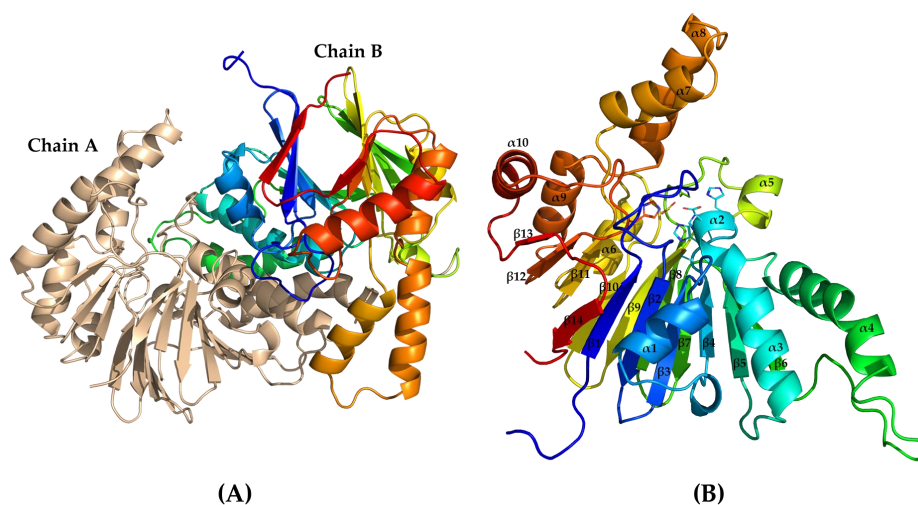


Figure 5. Cartoon representation of PaAst. (A) Dimer of PaAst. Chain A is colored in wheat and Chain B in rainbow color. (B) PaAst monomer. Side chains of the conserved Zn^{2+} -binding motifs are shown with lines.

Residues of the truncated recombinant PaAst were well defined in the electron density, with Chain B primarily presented hereafter for structural analysis (Figure 5B). The structure formed an MBL fold consisting of 14 β -strands (β 1- β 14) and 10 α -helices (α 1- α 10). The MBL fold exhibited a typical β -sandwich structure, and the two central β -sheets of it were constituted by 7 β -strands, respectively, β 7- β 13 and β 1- β 6 with β 14. The α -helices were decorated on either side of the β -sheets: α 1, α 2, α 3, and α 4 on one side, and α 5 to α 10 on the other.

Two neighboring high electron density peaks were identified at the core-facing end of the β -sandwich that modeled as metal ions; however, they were not determined as Zn ions corresponding to those in Yhfl. The residues nearby could constitute the metal ion-binding motifs strictly conserved in the MBL-fold proteins with one metal ion coordinated by His90, His92, His181, and Asp213, and the other coordinated by Asp94, His95, D213, and His289, according to the alignment with Yhfl (Figure 6). The metal-coordinating residues play critical roles as enzymatic active centers in MBL-fold hydrolases [4,18]. Attempts are underway to determine the metal ions by crystallization and enzymatic assays in the presence of metal ions, and site-directed mutations will be performed to further analyze its active center.

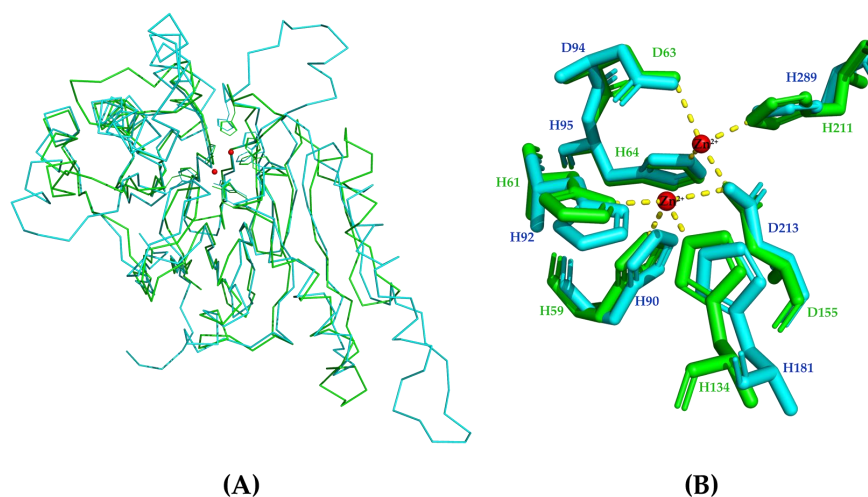


Figure 6. Structural alignment of PaAst and Yhfl (PDB: 6KNT, chain A). (A) Ribbon representation of PaAst and Yhfl. PaAst is in blue, Yhfl is in green, and Zn^{2+} is in red, and the side chains of metal ion binding sites are shown by lines. (B) Comparison of the metal ion binding sites. The metal ion binding site of PaAst is in blue, Yhfl is in green, and Zn^{2+} is in red.

Although several MBL-fold arylsulfatases have been reported in recent decades, limited knowledge could be obtained from their structures. In this study, our sequence and functional analyses revealed that PaAst is an arylsulfatase, and the specific activity, K_m and V_{max} of purified recombinant PaAst, was observed by 39.45 U/mg, 1.00 mM, and 60.80 U/mg at 50 °C, respectively. Its structure was determined at 2.0 Å and formed a dimer with MBL fold, which could be the first MBL-fold arylsulfatase reported with its structure determined. The identification and characterization of AtsA-like arylsulfatases had indicated the existence of MBL-fold arylsulfatases for years, and the structure of PaAst supported the classification of MBL-fold arylsulfatases as a novel type directly. This work provided insights into the MBL-fold arylsulfatases and may be the theoretical foundation for investigations into their catalytic mechanism.

3. Materials and Methods

3.1. Strains, Plasmids, and Reagents

PaAst (GenBank: ABG39403.1) was codon-optimized and synthesized by Sangon (Shanghai, China) with its N-terminal signal peptide truncated. The recombinant protein was cloned into a modified pET32a vector and expressed in *E. coli* BL21 (DE3) as

described previously, ligated by an N-terminal tobacco etch virus (TEV) cleavage site with the thioredoxin (Trx) and 6*His-tag for better solubility and purification [26,27].

PrimeSTAR[®] Max DNA Polymerase, T4 DNA Ligase, and the restriction enzymes were purchased from Takara Bio Inc. The Gel Extraction Kits and Plasmid Mini Kits were purchased from Omega Bio-tek (Norcross, GA, USA). All chemicals were in analytical grade and obtained commercially; for example, ampicillin sodium salt, isopropyl β -D-thiogalactoside (IPTG), imidazole, ethylenediaminetetraacetic acid (EDTA), and NiSO₄·6H₂O were purchased from Sangon, *p*NPS and *p*-nitrophenol (*p*NP) from Sigma-Aldrich (St. Louis, MO, USA), and the protein crystallization screening kits from Hampton Research (Aliso Viejo, CA, USA).

3.2. Sequence Analysis

Protein sequences were aligned by BLAST (<https://blast.ncbi.nlm.nih.gov/Blast.cgi>, accessed on 25 February 2023) and ESPript 3.0 (<http://esprict.ibcp.fr/ESPript/ESPript/>, accessed on 25 February 2023) [28]. The signal peptides and conserved domains were identified by SignalP-5.0 (<https://services.healthtech.dtu.dk/service.php?SignalP-5.0>, accessed on 13 September 2022) and NCBI Conserved Domain Search Service (CD Search) (<https://www.ncbi.nlm.nih.gov/Structure/cdd/wrpsb.cgi>, accessed on 15 September 2022), respectively [22,23]. The physical and chemical parameters of the protein were computed by ProtParam tool (<https://web.expasy.org/protparam/>, accessed on 24 March 2021).

3.3. Protein Expression and Purification

The recombinant PaAst-pET32a construct consisting of residues 23–328 was heterologously expressed in *E. coli* and purified by Ni²⁺-NTA resin affinity chromatography (GE Healthcare, Stockholm, Sweden) and size-exclusion chromatography (Superdex 200 increase 300 GL; GE Healthcare) successively [10,26,27]. The recombinant *E. coli* BL21 (DE3) cells containing *PaAst* gene were incubated at 37 °C and induced by IPTG (0.3 mM) at 16 °C for 12 h in Luria–Bertani medium. The protein was harvested via ultrasonication on ice in lysis buffer containing 50 mM Tris-HCl (pH 7.5) and 300 mM NaCl and centrifuged at 15,000 rpm for 15 min at 4 °C (Beckman Coulter, Brea, CA, USA).

Supernatant containing the fusion protein was loaded on a Ni²⁺-NTA resin affinity column to remove the non-specially bound proteins by elution buffer, which is lysis buffer with low concentrations of imidazole (20 mM and 40 mM), while the target protein could be eluted in a higher concentration of imidazole (300 mM). Digestion and dialysis were conducted at the same time with TEV Protease at 4 °C overnight for the cleavage of Trx-6*His-tag and removal of imidazole. Then a secondary Ni²⁺ affinity chromatography and size-exclusion chromatography were used to further purify the recombinant protein in buffer containing 50 mM Tris-HCl (pH 7.5) and 150 mM NaCl. The purification was evaluated by 15% SDS-PAGE, and the concentration of purified PaAst was determined using NanoDrop One (Thermo Scientific, Waltham, MA, USA).

3.4. Enzymatic Activity Assay

The enzymatic activity of PaAst was determined by the artificial substrate *p*NPS, which could be hydrolyzed into *p*NP and sulfate by arylsulfatases, as described [3,12,14]. A solution of both enzyme and substrate was made with 50 mM Tris-HCl (pH 7.5) buffer, and the reaction consisted of 20 μ L enzyme solution (0.23 μ g) and 80 μ L substrate solution. Moreover, the kinetic parameters were measured with *p*NPS in different concentrations (0.1, 0.5, 1, 1.5, 2, and 2.5 mM). After incubation at 50 °C for 8 min, the reaction was terminated by 20 μ L 1 M NaOH, and its absorbance at 410 nm was measured by a spectrophotometer to quantify the concentration of *p*NP and accordingly calculate the reacted *p*NPS. One unit of enzyme activity (U) was defined as the amount of enzyme required to degrade 1 μ M *p*NPS per min. The kinetic parameters of K_m and V_{max} were obtained by creating a Michaelis–Menten plot of reaction rate versus substrate concentrations using GraphPad Prism 8.2.1 [29].

3.5. Crystallization

The purified recombinant PaAst was concentrated to 10–15 mg/mL for crystallization, and the crystallization conditions were preliminary screened by the sitting-drop vapor-diffusion method in 96-well plates at 16 °C with more than ten commercial crystallization screening kits, for example, JCSG Core Suites (I to IV, and +, Molecular Dimensions) [10,26]. Crystals of the protein could be found in more than 70 reservoirs, composed of equal volumes (0.6 μ L) of protein solution and reservoir solutions, within 1 day. The diffraction-quality crystals were flash-frozen and kept in liquid nitrogen with cryoprotectant.

3.6. Structure Determination and Refinement

X-ray diffraction data sets for PaAst were collected at beamline BL18U1 of the Shanghai Synchrotron Radiation Facility (SSRF, Shanghai, China), and each contained 360 frames (oscillation range 1°). A complete data set was collected at 100 K from a single crystal of the protein obtained in 0.2 M sodium thiocyanate and 20% (*v/v*) PEG3350, and it was processed by HKL-2000 and XDS [30–32]. The structure of PaAst was determined by the molecular replacement method using Phaser with the crystal structure of metallo- β -lactamase fold protein YhfI from *Bacillus subtilis* (PDB: 6KNT) acting as the starting model [18,33]. Model building and refinement of the structure were executed by Coot and Phenix [34,35], respectively, and the final model was deposited in the Protein Data Bank with structure factors under an accession code of 8GYG (Table A1). The PyMOL Molecular Graphics System was used to visualize and analyze the protein structures.

Author Contributions: Conceptualization, P.D.; Formal analysis, W.Y., L.S. and H.Z.; Investigation, P.D., J.Y., L.W. and L.C.; Methodology, L.S.; Software, D.J.; Supervision, Y.W.; Visualization, W.Y.; Writing—original draft, P.D.; Writing—review and editing, W.Y. All authors have read and agreed to the published version of the manuscript.

Funding: This research was funded by the National Thousand Talents Program of China, Natural Science Foundation of Fujian Province (2019J01280 and 2021J01171), and Special Projects of the Central Government Guiding Local Science and Technology Development (2020L3008).

Data Availability Statement: Data of this study are available in the article.

Conflicts of Interest: The authors declare no conflict of interest.

Appendix A

Table A1. Diffraction data collection and refinement statistics of PaAst structure.

Parameter	Value(s)
Data collection	
Beamline	SSRF BL18U1
Wavelength (\AA)	0.97915
Space group	$P 1 2_1 1$
Unit cell parameters	
a, b, c (\AA)	55.17, 61.38, 89.60
α, β, γ ($^\circ$)	90, 97.88, 90
Resolution range (\AA)	38.61–1.55 (1.59–1.55)
Completeness (%)	99.7
No. of unique reflections measured	85,833
Redundancy	6.1 (6.5)
R_{merge}	0.117 (1.077)
$\langle I/\sigma(I) \rangle$	8.3 (1.8)
$CC_{1/2}$	0.995 (0.528)

Table A1. Cont.

Parameter	Value(s)
Refinement	
Resolution range (Å)	29.59–2.0
Completeness (%)	99.5
No. of unique reflections refined	40,070
R _{work} /R _{free} (%)	20.04/24.35
No. of molecules per asymmetric unit	2
No. of residues	Chain A: 291 Chain B: 305
No. of atoms	5202
Ramachandran Plot (%)	
Favored regions	97.63
Allowed regions	2.03
Outliers	0.34
Mean B value, overall (Å ²)	23.9
PDB ID	8GYG

Values in parentheses refer to the highest resolution shell.

Table A2. Purification yields of recombinant AtsA.

Purification Procedures	Total Protein (mg)	Total Activity (U)	Specific Activity (U/mg)	Purification Factor	Yield (%)
Crude extract	136.07	5000.57	36.75	1	100
Affinity chromatography	48.88	2099.67	42.96	1.17	41.98
Size-exclusion chromatography	6.39	500.15	78.32	2.13	10.00

Arylsulfatase AtsA was codon-optimized, synthesized, and heterologously expressed in *E. coli*. Enzymatic activities were determined by pNPS in 50 mM Tris-HCl (pH 7.5) buffer at 50 °C, the same as the conditions for PaAst.

References

- Pogorevc, M.; Faber, K. Purification and characterization of an inverting stereo- and enantioselective sec-alkylsulfatase from the gram-positive bacterium *Rhodococcus ruber* DSM 44541. *Appl. Environ. Microbiol.* **2003**, *69*, 2810–2815. [[CrossRef](#)] [[PubMed](#)]
- Long, M.; Ruan, L.; Li, F.; Yu, Z.; Xu, X. Heterologous expression and characterization of a recombinant thermostable alkylsulfatase (sdsAP). *Extremophiles* **2011**, *15*, 293–301. [[CrossRef](#)] [[PubMed](#)]
- Zhu, Y.; Liu, H.; Qiao, C.; Li, L.; Jiang, Z.; Xiao, A.; Ni, H. Characterization of an arylsulfatase from a mutant library of *Pseudoalteromonas carrageenovora* arylsulfatase. *Int. J. Biol. Macromol.* **2017**, *96*, 370–376. [[CrossRef](#)]
- Hagelueken, G.; Adams, T.M.; Wiehlmann, L.; Widow, U.; Kolmar, H.; Tummeler, B.; Heinz, D.W.; Schubert, W.D. The crystal structure of SdsA1, an alkylsulfatase from *Pseudomonas aeruginosa*, defines a third class of sulfatases. *Proc. Natl. Acad. Sci. USA* **2006**, *103*, 7631–7636. [[CrossRef](#)]
- Berteau, O.; Guillot, A.; Benjdia, A.; Rabot, S. A new type of bacterial sulfatase reveals a novel maturation pathway in prokaryotes. *J. Biol. Chem.* **2006**, *281*, 22464–22470. [[CrossRef](#)]
- Sogi, K.M.; Gartner, Z.J.; Breidenbach, M.A.; Appel, M.J.; Schelle, M.W.; Bertozzi, C.R. *Mycobacterium tuberculosis* Rv3406 is a type II alkyl sulfatase capable of sulfate scavenging. *PLoS ONE* **2013**, *8*, e65080. [[CrossRef](#)]
- Muller, I.; Kahnert, A.; Pape, T.; Sheldrick, G.M.; Meyer-Klaucke, W.; Dierks, T.; Kertesz, M.; Uson, I. Crystal structure of the alkylsulfatase AtsK: Insights into the catalytic mechanism of the Fe(II) alpha-ketoglutarate-dependent dioxygenase superfamily. *Biochemistry* **2004**, *43*, 3075–3088. [[CrossRef](#)] [[PubMed](#)]
- Kahnert, A.; Kertesz, M.A. Characterization of a sulfur-regulated oxygenative alkylsulfatase from *Pseudomonas putida* S-313. *J. Biol. Chem.* **2000**, *275*, 31661–31667. [[CrossRef](#)]
- Davison, J.; Brunel, F.; Phanopoulos, A.; Prozzi, D.; Terpstra, P. Cloning and sequencing of *Pseudomonas* genes determining sodium dodecyl sulfate biodegradation. *Gene* **1992**, *114*, 19–24. [[CrossRef](#)]
- Sun, L.; Chen, P.; Su, Y.; Cai, Z.; Ruan, L.; Xu, X.; Wu, Y. Crystal structure of thermostable alkylsulfatase SdsAP from *Pseudomonas* sp. S9. *Biosci. Rep.* **2017**, *37*, BSR20170001. [[CrossRef](#)]
- Knaus, T.; Schober, M.; Kepplinger, B.; Faccinelli, M.; Pitzer, J.; Faber, K.; Macheroux, P.; Wagner, U. Structure and mechanism of an inverting alkylsulfatase from *Pseudomonas* sp. DSM6611 specific for secondary alkyl sulfates. *FEBS J.* **2012**, *279*, 4374–4384. [[CrossRef](#)] [[PubMed](#)]
- Kim, D.E.; Kim, K.H.; Bae, Y.J.; Lee, J.H.; Jang, Y.H.; Nam, S.W. Purification and characterization of the recombinant arylsulfatase cloned from *Pseudoalteromonas carrageenovora*. *Protein Expr. Purif.* **2005**, *39*, 107–115. [[CrossRef](#)] [[PubMed](#)]

13. Zhu, Y.; Liang, M.; Li, H.; Ni, H.; Li, L.; Li, Q.; Jiang, Z. A mutant of *Pseudoalteromonas carrageenovora* arylsulfatase with enhanced enzyme activity and its potential application in improvement of the agar quality. *Food Chem.* **2020**, *320*, 126652. [[CrossRef](#)]
14. Jung, K.T.; Kim, H.W.; You, D.J.; Nam, S.W.; Kim, B.W.; Jeon, S.J. Identification of the first archaeal arylsulfatase from *Pyrococcus furiosus* and its application to desulfatation of agar. *Biotechnol. Bioprocess Eng.* **2013**, *17*, 1140–1146. [[CrossRef](#)]
15. Shahbazi, R.; Kasra-Kermanshahi, R.; Gharavi, S.; Moosavi-Nejad, Z.; Borzooee, F. Screening of SDS-degrading bacteria from car wash wastewater and study of the alkylsulfatase enzyme activity. *Iran. J. Microbiol.* **2013**, *5*, 153–158. [[PubMed](#)]
16. Zhang, C.; An, D.; Xiao, Q.; Chen, F.Q.; Zhang, Y.H.; Weng, H.F.; Xiao, A.F. Convenient Agarose Preparation with Hydrogen Peroxide and Desulfation Process Analysis. *Mar. Drugs* **2021**, *19*, 297. [[CrossRef](#)] [[PubMed](#)]
17. Xu, X.; Deng, X.; Lin, J.; Yang, J. Characterization and substrate-accelerated thermal inactivation kinetics of a new serine-type arylsulfatase. *Enzyme Microb. Technol.* **2022**, *154*, 109961. [[CrossRef](#)] [[PubMed](#)]
18. Na, H.W.; Namgung, B.; Song, W.S.; Yoon, S.I. Structural and biochemical analyses of the metallo-beta-lactamase fold protein YhfI from *Bacillus subtilis*. *Biochem. Biophys. Res. Commun.* **2019**, *519*, 35–40. [[CrossRef](#)]
19. Kertesz, M.A. Riding the sulfur cycle—metabolism of sulfonates and sulfate esters in gram-negative bacteria. *FEMS Microbiol. Rev.* **2000**, *24*, 135–175. [[CrossRef](#)]
20. Duvaud, S.; Gabella, C.; Lisacek, F.; Stockinger, H.; Ioannidis, V.; Durinx, C. ExPasy, the Swiss Bioinformatics Resource Portal, as designed by its users. *Nucleic Acids Res.* **2021**, *49*, W216–W227. [[CrossRef](#)]
21. Almagro Armenteros, J.J.; Tsirigos, K.D.; Sonderby, C.K.; Petersen, T.N.; Winther, O.; Brunak, S.; von Heijne, G.; Nielsen, H. SignalP 5.0 improves signal peptide predictions using deep neural networks. *Nat. Biotechnol.* **2019**, *37*, 420–423. [[CrossRef](#)] [[PubMed](#)]
22. Marchler-Bauer, A.; Bo, Y.; Han, L.; He, J.; Lanczycki, C.J.; Lu, S.; Chitsaz, F.; Derbyshire, M.K.; Geer, R.C.; Gonzales, N.R.; et al. CDD/SPARCLE: Functional classification of proteins via subfamily domain architectures. *Nucleic Acids Res.* **2017**, *45*, D200–D203. [[CrossRef](#)] [[PubMed](#)]
23. Lu, S.; Wang, J.; Chitsaz, F.; Derbyshire, M.K.; Geer, R.C.; Gonzales, N.R.; Gwadz, M.; Hurwitz, D.I.; Marchler, G.H.; Song, J.S.; et al. CDD/SPARCLE: The conserved domain database in 2020. *Nucleic Acids Res.* **2020**, *48*, D265–D268. [[CrossRef](#)]
24. Holm, L. Dali server: Structural unification of protein families. *Nucleic Acids Res.* **2022**, *50*, W210–W215. [[CrossRef](#)] [[PubMed](#)]
25. Pellegrini, O.; Li de la Sierra-Gallay, I.; Piton, J.; Gilet, L.; Condon, C. Activation of tRNA maturation by downstream uracil residues in *B. subtilis*. *Structure* **2012**, *20*, 1769–1777. [[CrossRef](#)]
26. Zhu, C.; Chen, Y.; Isupov, M.N.; Littlechild, J.A.; Sun, L.; Liu, X.; Wang, Q.; Gong, H.; Dong, P.; Zhang, N.; et al. Structural Insights into a Novel Esterase from the East Pacific Rise and Its Improved Thermostability by a Semirational Design. *J. Agric. Food Chem.* **2021**, *69*, 1079–1090. [[CrossRef](#)]
27. Yang, W.; Sun, L.; Dong, P.; Chen, Y.; Zhang, H.; Huang, X.; Wu, L.; Chen, L.; Jing, D.; Wu, Y. Structure-guided rational design of the *Geobacillus thermoglucosidasius* feruloyl esterase GthFAE to improve its thermostability. *Biochem. Biophys. Res. Commun.* **2022**, *600*, 117–122. [[CrossRef](#)]
28. Robert, X.; Gouet, P. Deciphering key features in protein structures with the new ENDscript server. *Nucleic Acids Res.* **2014**, *42*, W320–W324. [[CrossRef](#)]
29. Mitteer, D.R.; Greer, B.D.; Randall, K.R.; Briggs, A.M. Further Evaluation of Teaching Behavior Technicians to Input Data and Graph Using GraphPad Prism. *Behav. Anal.* **2020**, *20*, 81–93. [[CrossRef](#)]
30. Minor, W.; Cymborowski, M.; Borek, D.; Cooper, D.R.; Chruszcz, M.; Otwinowski, Z. Optimal structure determination from sub-optimal diffraction data. *Protein Sci.* **2022**, *31*, 259–268. [[CrossRef](#)]
31. Otwinowski, Z.; Minor, W. Processing of X-ray diffraction data collected in oscillation mode. *Methods Enzymol.* **1997**, *276*, 307–326. [[CrossRef](#)]
32. Kabsch, W. Xds. *Acta Crystallogr. D Biol. Crystallogr.* **2010**, *66*, 125–132. [[CrossRef](#)] [[PubMed](#)]
33. McCoy, A.J.; Grosse-Kunstleve, R.W.; Adams, P.D.; Winn, M.D.; Storoni, L.C.; Read, R.J. Phaser crystallographic software. *J. Appl. Crystallogr.* **2007**, *40*, 658–674. [[CrossRef](#)] [[PubMed](#)]
34. Emsley, P.; Cowtan, K. Coot: Model-building tools for molecular graphics. *Acta Crystallogr. D Biol. Crystallogr.* **2004**, *60*, 2126–2132. [[CrossRef](#)] [[PubMed](#)]
35. Adams, P.D.; Afonine, P.V.; Bunkoczi, G.; Chen, V.B.; Davis, I.W.; Echols, N.; Headd, J.J.; Hung, L.W.; Kapral, G.J.; Grosse-Kunstleve, R.W.; et al. PHENIX: A comprehensive Python-based system for macromolecular structure solution. *Acta Crystallogr. D Biol. Crystallogr.* **2010**, *66*, 213–221. [[CrossRef](#)] [[PubMed](#)]

Disclaimer/Publisher’s Note: The statements, opinions and data contained in all publications are solely those of the individual author(s) and contributor(s) and not of MDPI and/or the editor(s). MDPI and/or the editor(s) disclaim responsibility for any injury to people or property resulting from any ideas, methods, instructions or products referred to in the content.